Noble-gas bubbles in metals: Molecular-dynamics simulations and positron states

Kjeld O. Jensen*

Metallurgy Department, Risø National Laboratory, DK-4000 Roskilde, Denmark

R. M. Nieminen[†]

Department of Physics, University of Jyväskylä, SF-40100 Jyväskylä, Finland
(Received 3 April 1987)

A theoretical treatment of atomic structure and positron states in noble-gas bubbles in metals is presented. The Al-He and Cu-Kr systems are considered as specific examples. For large bubbles (radii above a few tens of angstroms) a calculational scheme is developed combining molecular-dynamics results for the metal–noble-gas interface with positron calculations. It is demonstrated that a positron is trapped at the surface of a noble-gas bubble, i.e., at the metal-gas interface. The annihilation rate with metal electrons is similar to that at a clean surface, while simultaneously there is a significant annihilation rate with gas-atom electrons. This enables relationships between the gas density and the positron lifetime to be obtained for the systems considered. Experimental evidence supports the theoretical relations. In the molecular-dynamics simulations a trend towards close-packed layer-by-layer ordering of the gas atoms close to the metal-gas interface is found even in the cases where the bulk gas is in a fluid phase. The positron-state calculations also cover the case of adsorbed noble-gas layers at surfaces. For vacancy–noble-gas clusters containing up to 13 vacancies complementary positron results obtained with the calculational method developed by Puska and Nieminen are presented.

I. INTRODUCTION

The behavior of noble gases in metals has attracted considerable interest in recent years. This interest has mainly been triggered by the materials problems (embrittlement) in fusion reactor materials associated with generation of helium,[1] while more fundamental issues are also increasingly being addressed.[2] Bombardment with heavy noble-gas ions is widely used in various preparation processes for metal surfaces and films, e.g., sputter cleaning[3] and ion-beam mixing.[4] Thus, motivation from a materials science point of view for studies of noble gases in metals exists not only for He but also for the other rare gases. Noble gases are practically insoluble in metals and therefore show a strong tendency to precipitate into what are conventionally called bubbles even in the cases where the precipitate is in a solid phase. To evaluate the effects of noble gases on physical or materials properties of metals, it is therefore important to be able to characterize noble-gas bubbles and to develop an understanding of their behavior. Numerous techniques have been applied to this end including, primarily in more recent years, the positron-annihilation technique[5−10] (PAT), now well established in the study of vacancy-type defects and their interactions in solids.[11,12]

The possibility of the positron lifetime as a signature of the gas density inside bubbles has been considered earlier.[7,13] However, in previous studies no detailed account of the positron behavior in gas bubbles was made and the proposed relationships between gas density and positron lifetime therefore lacked a firm basis. The purpose of the present work is to provide a theoretical foundation for the interpretation of the PAT results and to derive relations between positron lifetime and gas density for a selection of metal noble-gas systems, thus demonstrating the potential use of PAT to determine gas densities in bubbles. Other methods have been used to address the gas density problem, but so far unambiguous density determination has been problematic.[14]

The results presented in this paper are part of a more general study with the aim to obtain a better understanding of PAT results for metals containing noble-gas bubbles. This study also incorporates PAT experiments performed on He bubbles in Al (Ref. 6) and Kr bubbles in Cu and Ni.[9,10] This motivates the choice of the Al-He and Cu-Kr systems as specific applications of the general calculational method developed for metal noble-gas systems. A short account of the Al-He calculations has been published previously.[15]

Our results demonstrate that in large bubbles (radii above ~10 Å) the positron is trapped at the bubble surface, i.e., at the gas-metal interface. To determine the positron characteristics it is necessary to know the atomic structure close to the interface. This information is obtained by sets of molecular-dynamics[16] (MD) simulations for Al-He and Cu-Kr interfaces. The MD method was applied earlier to He-filled platelets[17] and small He-vacancy clusters,[18] but to our knowledge no metal noble-gas interface results have been published previously.

Calculations for positrons trapped in small vacancy gas clusters will also be presented, supplementing the interface results applicable to large bubbles.

This paper is organized as follows: Section II contains the results for the Al-He system and presents the general calculational approach applied. The results for the Cu-Kr system are presented separately in Sec. III. The re-

sults are discussed in Sec. IV. Section V provides a summary and conclusion.

II. METHODS AND RESULTS: Al-He

A. Molecular-dynamics simulations

In general, large gas bubbles (radii larger than a few tens of angstroms) have three-dimensional faceted shapes. The problem of describing the atomic structure at the bubble surface can therefore be approached by considering a planar metal noble-gas interface representing the facets. The interface simulations were performed with the molecular-dynamics program MOLDY originally developed by Finnis and Harker.[19] For the Al-He system a sandwich geometry was applied with six layers of Al atoms [(001) planes] containing in total 192 atoms separating two sets of up to 300 He atoms in a box of constant volume with periodic boundary conditions in all three dimensions. The He atoms were initially arranged in a regular array. However, any information about the initial He positions was rapidly lost as the simulation proceeded.

The interatomic He-He potential was that of Aziz et al.[20] This potential is known to give a good description of high-density He fluids.[21] The potential was truncated at a He-He distance of 5 Å.

The major requirement for the He-Al interaction potential is that it yields the correct potential for the He atoms near the Al surface, when contributions from all metal atoms are added for each He atom. The Al-He potential is a sum of two parts:

$$V_{Al-He}(\mathbf{r}) = V_{EM}(\mathbf{r}) + V_{vdW}(\mathbf{r}) . \tag{2.1}$$

The primary contribution to the He-Al interaction is the repulsive part V_{EM}. This is described by the effective medium formula[22]

$$V_{EM}(\mathbf{r}) = \alpha_{eff} n_{el}(\mathbf{r}) , \tag{2.2}$$

where $n_{el}(\mathbf{r})$ is the atomic electron density of the metal atom and $\alpha_{eff} = 255$ eV a_0^3. Equation (2.2) stems from the linear relationship[22] between the (kinetic-) energy repulsion and electron density, and from the assumption that the surface-electronic density can be described by a superposition of atomic densities. This is known to be a good approximation for a flat surface.[23]

At a metal surface there is an additional contribution to the He potential—namely the (weak) van der Waals attraction, which is asymptotically proportional to $(z-z_0)^{-3}$, where z is the He-surface distance and z_0 a constant.[24] Below we choose $z=0$ to coincide with the outermost Al layer with He occupying the space $z > 0$. In order to obtain the van der Waals potential as a sum of pairwise interactions, the interatomic potential included an attractive term

$$V_{vdW}(r) = -C(r-r_1)^{-6}f(r-r_1) , \tag{2.3}$$

where the cutoff function $f(r-r_1)$ is given by

$$f(r-r_1) = 1 - [2x(1+x)+1]\exp(-2x) ,$$

$$x = [k(r-r_1)]^2 . \tag{2.4}$$

The constants $C = 7.27$ eV Å^6, $r_1 = 0.55$ Å, and $k = 0.567$ Å^{-1} are adjusted so as to give a physisorption well of depth ~ 5 meV at a distance 4 Å from the surface.[25] The shape of the well agrees well with the universal shape for noble-gas potentials at solid surfaces proposed by Vidali et al.[26] The cutoff function $f(r-r_1)$ ensures that the repulsive part of the He-surface potential for $z < 4$ Å is essentially unaffected by the inclusion of V_{vdW} in the potential. The truncation radius for the He-Al potential was chosen as 8 Å.

A Morse potential[27] truncated at 7 Å was used for the Al-Al pairwise interactions. The parameters entering the potential were fitted to reproduce bulk Al properties (lattice constant, bulk modulus, and sublimation energy). More advanced descriptions of metal-metal interactions exist,[28] but for the present application a simple potential like the Morse potential is adequate since the primary objective is to study the arrangement of the gas rather than the metal atoms. The latter basically provide the substrate against which the fluid is pressed. In the region of space sampled by the gas atoms in the simulations, the potential acting on the gas due to the metal surface stems almost entirely from the outermost layer of metal atoms, and the corrugation of the potential parallel to the surface is small. This means that inaccuracies in the detailed relaxations of the metal atoms do not have any significant impact on the gas-density profiles.

The simulations were run for up to 1200 time steps of 5×10^{-15} s. First, the system was equilibrated to the temperature T required, this being 300 K in most cases. Thereafter, the time-averaged density profile $n_{He}(z)$ perpendicular to the interface was calculated using z bins of ~ 0.1 Å. The two sides of the "sandwich" were combined into one profile. Two examples are shown in Fig. 1. With increasing mean He density $\bar{n}_{He}$ defined as the average value for large z, a strong peak in the He density profile first develops near the Al surface and secondary peaks in the fluid follow. The surface peak is not associated with the physisorption well in the He-Al interaction (it also appears when no attractive part is included in the He-Al potential). Instead it originates from statistical packing of atoms next to the repulsive metal surface, much as with hard spheres near an impenetrable wall.[29] The other peaks appearing at higher densities signal incipient ordering in the compressed fluid. The distance between peaks corresponds to that between close-packed planes at a given $\bar{n}_{He}$. The peaks in the density profiles are reminiscent of the layered structure observed in simulations of He-filled platelets in Mo.[17] The presence of the He surface layer indicated by the density profiles can also be seen in the trajectory plot in Fig. 2 corresponding to the profile in Fig. 1(b). Figure 2 shows that the He atoms are quite mobile even when the time-averaged density profile demonstrates a division into layers. No appreciable enhancement of the lateral ordering is observed in the He layer closest to the interface com-
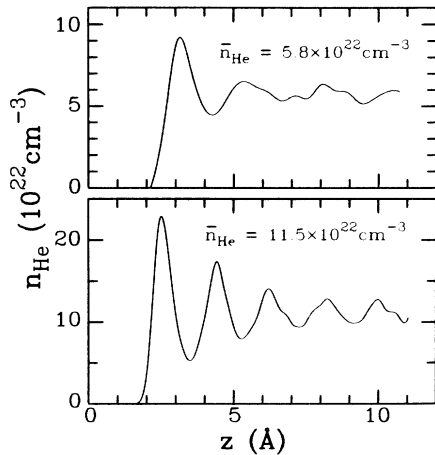
FIG. 1. One-dimensional He density profiles perpendicular to the Al(001) surface obtained by molecular-dynamics simulations. The outermost Al layer is at $z = 0$. The mean He densities, $\bar{n}_{He}$, indicated are the average values for large z. The simulation temperature was in both (a) and (b) 300 K. The profiles have been averaged over 500 time steps (2.5 ps) after equilibrium was attained.

pared to the deeper layers representing the bulk structure. Lateral corrugations of the distribution of He atoms near the metal are only detectable at the highest densities and are in all cases weak.

B. Positron surface-state calculations: Ordered He layers

For large, empty voids in aluminum the lowest-energy positron state is the surface state.[30] From the present calculations (see below) we find that the surface (interface) state remains the most stable also in He-containing cavities (bubbles) for all values of the He density inside the bubble. In the positron calculations we first consider an Al(001) surface with He atoms outside the surface ordered in various geometries to be described. The calculations are based on an extension of the corrugated mir-
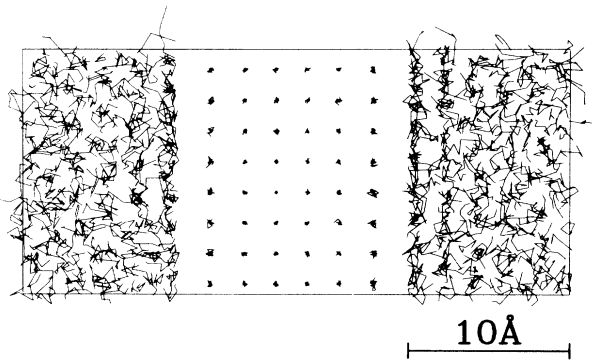

FIG. 2. Molecular-dynamics trajectory plot for an Al-He interface, $\bar{n}_{He} = 11.5 \times 10^{22}$ cm^{-3}, $T = 300$ K. The six central planes are comprised of Al atoms; the remaining atoms are He. The plot covers a time span of 1 ps (200 time steps). The reentry at the opposite face, as required by the periodic boundary conditions, of an atom leaving the box at one face is not taken into account in drawing the plot.

ror model of Nieminen and Puska,[31] where the positron surface state is described as an image-potential-induced state.

The effective potential V^+ acting on the positron contains electrostatic and correlation parts which are taken as sums of metal and He contributions:

$$V^+(\mathbf{r}) = V^+_{met}(\mathbf{r}) + \sum_{\mathbf{R}} V^+_{He}(\mathbf{r} - \mathbf{R}) . \tag{2.5}$$

Above, $\mathbf{R}$ denotes summation over the gas-atom positions. Because of the inertness and low polarizability of He the metal-positron interaction is only negligibly screened by the He atoms and is well approximated by the positron potential V^+_{met} at a clean metal surface (consisting of Coulomb and correlation parts, the latter including the image potential).[31] For positron-surface distances z larger than ~ 2 Å only the long-range image interaction survives. Thus, the model assumes the positron screening charge to reside at the metal surface and there is no accumulation of electrons around the positron for $z > 2$ Å. Since the MD simulations have shown that the He atoms very rarely get closer than this to the surface (cf. Fig. 1), this also means that the metal electrons only weakly screen the positron-He interactions. Therefore we include in V^+_{He} both the atomic Coulomb potential V_C^+ and the (long-range) polarization potential[32] V^+_{pol}:

$$V^+_{He}(\mathbf{r}) = V_C^+(\mathbf{r}) + V^+_{pol}(\mathbf{r}) . \tag{2.6}$$

The latter is given by

$$V^+_{pol}(\mathbf{r}) = \begin{cases} -\alpha/2r^4, & r \geq r_0 \\ -\alpha/2r_0^4, & r < r_0 \end{cases} \tag{2.7}$$

where α is the static dipole polarizability and r_0 an adjustable length parameter. As in calculations for bulk He values of $\alpha = 1.383a_0^3$ and $r_0 = 1.57a_0$ were used;[13,32] these reproduce the correct positron-helium scattering length.

We obtain the ground-state wave function from a numerical solution to the three-dimensional Schrödinger equation with the potential given by Eq. (2.5). Calculated positron wave functions for the clean Al(001) surface and for a surface covered with a single monolayer of He are shown in Fig. 3. This demonstrates the important result that the surface state remains stable with the He present: the overlayer disturbs the wave function only locally near each He nucleus.

The positron and electron densities (electronic densities are calculated by superimposing atomic densities) are used to calculate the positron annihilation rate λ. This rate is divided into contributions from gas-atom (He) electrons, λ_{gas}, and metal (Al) electrons, λ_{met}, i.e.,

$$\lambda = \lambda_{gas} + \lambda_{met} . \tag{2.8}$$

Both rates are proportional to the overlap of the two densities, multiplied by an enhancement factor, which depends on the nature of the annihilating electrons. For λ_{gas} from tightly bound electrons one can apply the independent-particle description with a constant enhancement factor[33] γ:
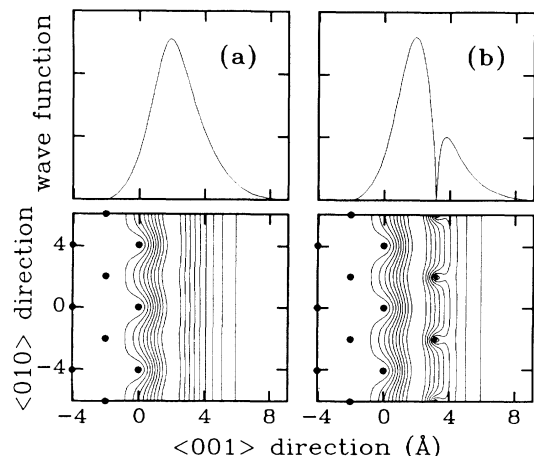
FIG. 3. Positron wave functions at (a) a clean Al(001) surface and (b) Al(001) with one monolayer of He at fourfold sites shown as contour plots (lower panels) and cross sections through a fourfold site (upper pannels). The solid dots denote positions of Al atoms in the plane of the figure. The He positions in (b) correspond to the dips in the wave function ~ 3 Å from the surface. The wave functions in (a) and (b) are both normalized within the unit cell and contour spacings are $\frac{1}{10}$ of the maximum value in each case.

$$\lambda_{gas} = \pi r_e^2 c \gamma \int d\mathbf{r} \, | \, \psi_+(\mathbf{r}) \, |^2 \rho(\mathbf{r}) \, , \tag{2.9}$$

where ψ_+ is the positron wave function, ρ the gas-atom electron density, r_e the classical electron radius, and c the speed of light. In the case of He (λ_{gas} denoted by λ_{He}) we apply a value of 2.9 for γ. This is the γ required to reproduce the experimental annihilation rate versus He-density relation for bulk He.[13] The calibration of λ_{gas} against bulk measurements is justified by the lack of screening of the positron-He interaction inferred above.

Similarly, λ_{met} is the result of the positron-metal electron overlap.[31,34] For all geometries considered, the calculations show that the λ_{met} value for Al (λ_{Al}) can be approximated accurately by the value for a bare Al(001) surface since only in a small volume (radius ~ 0.5 Å) around each He atom does the positron wave function deviate substantially from the wave function at the clean surface (see Fig. 3). The deviation will therefore primarily be in the image-potential region, where the positron-electron overlap vanishes.

It is, however, not straightforward to obtain an accurate, absolute value for λ_{Al} theoretically.[34] This is due to the difficulty in accounting for the electron accumulation around the positron in the transition region going from the local screening behavior close to the surface to the image-potential region far from the surface where no accumulation occurs. The obvious alternative is to use an empirical λ_{Al}. The most direct determination of λ_{Al} for a clean Al surface has been made in a positron-beam experiment.[35] The value, $\lambda_{Al} = 1.72$ ns^{-1}, however, deviates from the annihilation rate associated[36] with nominally empty voids in Al, $\lambda_{Al} = 2.0-2.2$ ns^{-1}. Since continuity between positron lifetimes for bubbles with finite He density and voids with $\bar{n}_{He} = 0$ is desirable, we use

$\lambda_{Al} = 2.0$ ns^{-1} to compute numerical values for the lifetime, $\tau = (\lambda_{Al} + \lambda_{He})^{-1}$. Note that only at the instant where τ is calculated does the actual value of λ_{Al} play a role. Otherwise the results, notably λ_{He} and the dependence on the fluid density, are independent of the absolute value of λ_{Al}.

Computational convenience imposes a requirement of relatively high symmetry on the calculations. Thus, geometries with irregular He positions such as those obtained from the MD simulations cannot be treated directly. Instead, the combination of MD and positron calculations (Sec. II C) will be made through an intermediate step where we first treat positron surface states on Al(001) with various configurations of *ordered* He overlayers.

Figure 4 shows the binding energy E_b of the positron (with respect to vacuum) as a function of the He-surface distance z_{He} for single layers of He at fourfold sites at coverages $\Theta = 1$, 0.5 [$c(2 \times 2)$ structure], and 0.25 [$p(2 \times 2)$]. Note that E_b *increases* compared to the clean surface value, $E_b^0 = 2.84$ eV. The energy gain arising from the positron-He correlation thus more than compensates for the increase in kinetic energy due to the depletion of the positron wave function around the helium nuclei. Figure 5 shows the corresponding values for the annihilation rate λ_{He}. Test calculations have shown that the results in Figs. 4 and 5 also hold if the He atoms are placed on lattice sites (i.e., on top of surface atoms) instead of fourfold sites, which indicates that corrugation effects parallel to the surface have little effect on λ_{He} and E_b.

It is seen from Fig. 5 that, for any z_{He}, λ_{He} is proportional to the coverage (this holds up to an unphysically high coverage of 2, i.e., when both lattice and fourfold sites are occupied). We find a related result also when the He is not confined to a single layer, since in calculations with several $c(2 \times 2)$ layers at different z_{He} (chosen to give a coarse-grained representation of the MD He profiles) λ_{He} is found to be identical—within numerical
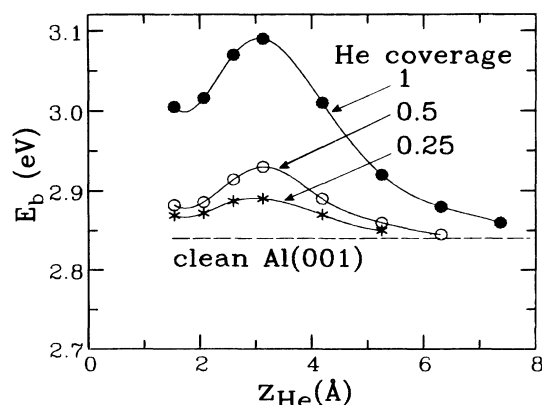

FIG. 4. Binding energy with respect to vacuum of a positron at an Al(001) surface covered by a single He layer as a function of the surface-He distance. The He coverage is indicated for each set of results. The clean Al(001) binding energy is indicated as the horizontal dashed line.
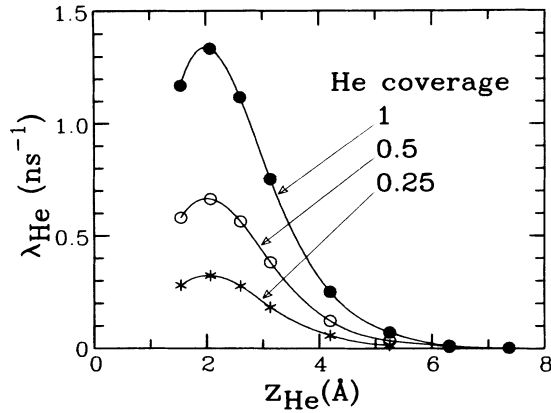
FIG. 5. Annihilation rates with He electrons for the same systems as included in Fig. 4.

accuracy—to the λ_{He} obtained by summing contributions from the individual layers using the single-layer results in Fig. 5. These observations indicate that each He atom contributes *additively* to λ_{He} and that the detailed geometric arrangement (i.e., the degree of ordering) of He atoms at a given distance from the interface is unimportant for the annihilation characteristics. This is related to the fact mentioned above that the He atoms only very locally perturb the positron wave function. The experimentally observed[37] proportionality between positron annihilation rate and gas density for bulk He is another manifestation of this effect.

C. Positron results for the Al-He interface

In this subsection we consider only the Al(001) surface explicitly. However, since both the positron-metal and He-metal potentials are nearly identical for the low-index Al surfaces, this implies little loss of generality. The results should therefore be applicable to a general
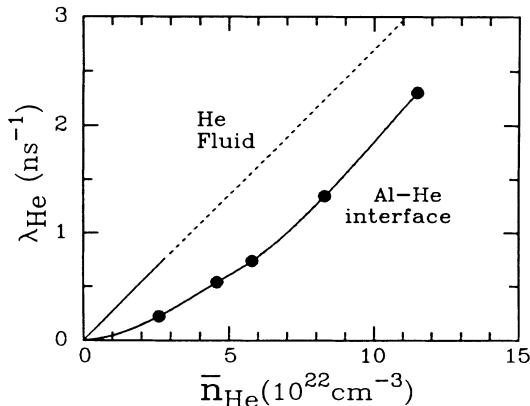

FIG. 6. Annihilation rates with He electrons as function of He density for a positron trapped at an Al-He interface (solid circles). A spline function is drawn between the points. For comparison, the corresponding relation for bulk He fluid is shown. The end of the solid line indicates the limit of the experimental results for the bulk fluid (Ref. 37). The dashed line is a linear extrapolation of the experimental relation.
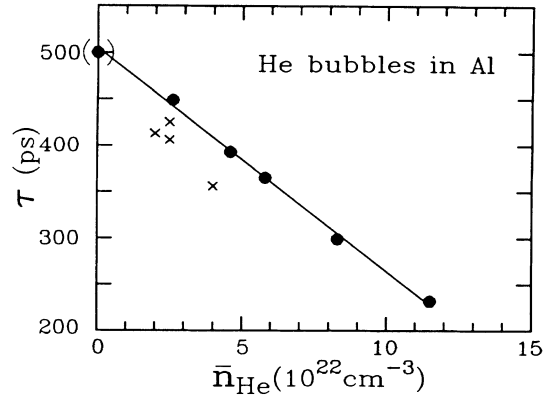

FIG. 7. Lifetime for a positron trapped by a He bubble in Al vs He density inside the bubble. Solid circles denote theoretical interface results with $\lambda_{Al} = 2.0$ ns^{-1} (see text). The line drawn is a visual fit. The crosses are based on experimental data with densities estimated by the thermal-equilibrium condition (see text).

Al surface encountered in a large He bubble.

The additivity of λ_{He} (see Sec. II B) will permit one to calculate the λ_{He} for a positron trapped at a He-Al interface without having to solve the positron Schrödinger equation for the specific geometry. The procedure is to find the contribution from each part (i.e., z bin) of the He profile individually using the single-layer results (Fig. 5) and subsequently add contributions from all parts of the profile to obtain the total λ_{He}. One can apply the formula

$$\lambda_{He} = \sum_i \Theta(z_i)\lambda_{He}^1(z_i) . \tag{2.10}$$

Here, z_i is the distance from the metal surface to the ith interval used in the MD calculation of the He-density profile. The He density within each interval is converted into a relative coverage denoted by $\Theta(z_i)$ as $\Theta(z_i) = n_{He}(z_i)\Delta z/c_0$, where Δz is the bin size and c_0 is the two-dimensional density corresponding to unit coverage [1.22×10^{15} cm^{-2} for Al(001)]. The proportionality constant between λ_{He} and Θ for each interval is given by the $\Theta = 1$ curve in Fig. 5, $\lambda_{He}^1(z)$. Figure 6 shows calculated values of λ_{He} for different values of $\bar{n}_{He}$. One observes that λ_{He} increases more than linearly with $\bar{n}_{He}$, because as the He density increases the He profile is
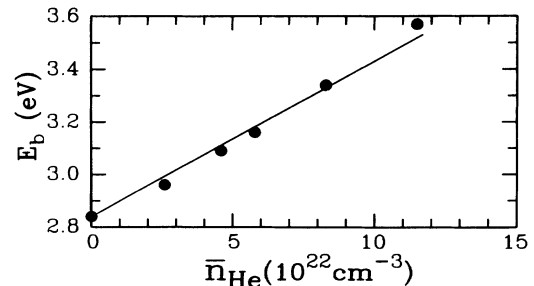

FIG. 8. Calculated binding energy (with respect to vacuum) of a positron trapped at an Al-He interface as function of the He density.

pressed closer to the metal surface, resulting in a larger positron-He overlap. For comparison also the λ_{He}-n_{He} relation for bulk helium[13,37] is shown in Fig. 6. Figure 7 displays the lifetimes, $\tau=(\lambda_{\text{Al}}+\lambda_{\text{He}})^{-1}$, calculated with the λ_{He} values from Fig. 6 and $\lambda_{\text{Al}}=2.0$ ns^{-1}. Figure 7 demonstrates a nearly linear relationship between τ and $\bar{n}_{\text{He}}$. The line in Fig. 7 corresponds to a linear fit:

$$\tau(\text{ps})=500-23.5\bar{n}_{\text{He}}(10^{22}\text{ cm}^{-3}) . \qquad (2.11)$$

If one applies a similar additivity procedure for the energy difference, $\Delta E_b=E_b-E_b^0$, the binding energies of the positron at the He-Al interface can be estimated. The explicit calculations for the positron do not justify this approach to the same degree for ΔE_b as for λ_{He} (as can be seen in Fig. 4, ΔE_b for single He layers is not perfectly proportional to the coverage). However, a first estimate of E_b can be obtained. We find that ΔE_b is approximately proportional to $\bar{n}_{\text{He}}$ and reaches 0.7 eV at $\bar{n}_{\text{He}}=11.5\times10^{22}$ cm^{-3} (see Fig. 8). Simultaneously, positronium (Ps) formation, the ordinary desorption channel for a surface-trapped positron,[38] is rendered less favorable also because of the mainly repulsive Ps-He interaction.[39] The helium thus serves to stabilize the positron surface state. This is not surprising since the positron-He interaction is dominantly attractive at the densities considered here, as demonstrated by the clustering of He around the positron at low temperatures in fluid He.[37] To get the positron binding energy to a He bubble with respect to the positron bulk state in Al, the positron work function, which for Al(001) is -0.19 eV (Ref. 38), should be subtracted from the E_b values in Fig. 8. The variation of E_b with $\bar{n}_{\text{He}}$ infers[40] that the specific trapping rate of positrons into He bubbles, μ, varies with $\bar{n}_{\text{He}}$. Considering electron-hole–pair–mediated trapping, the relative variation of μ is predicted[40] to be of the same order as the relative variations in E_b, i.e., presumably deviating at most $\sim30\%$ from the empty-void value ($\bar{n}_{\text{He}}=0$).

For $T=100$ K a single MD run was made at $\bar{n}_{\text{He}}=5.8\times10^{22}$ cm^{-3}. The He-density profile resembles that for $T=300$ K at the same $\bar{n}_{\text{He}}$ [Fig. 1(a)], only shifted a few tenths of angstroms from the metal surface. This shift reduces the positron-He overlap slightly and the calculated lifetime of 381 ps is about 20 ps higher than the 300-K value.

A single calculation for the Cu-He interface was carried out along the same lines as the Al-He calculations. For $\bar{n}_{\text{He}}=8.5\times10^{22}$ cm^{-3} we get $\lambda_{\text{He}}=1.36$ ns^{-1} (with $\lambda_{\text{Cu}}=2$ ns^{-1}, this gives $\tau=298$ ps) and $\Delta E_b=0.48$ eV, in striking agreement with the Al results (cf. Figs. 6–8). The source of this agreement is discussed in Sec. IV A.

D. Comparison with experiment

The crosses in Fig. 7 represent experimental results[6] for Al samples where 30–100 ppm (sample-dependent) He was introduced by (600–800)-MeV proton irradiation. The lifetimes are those of the most long-lived component in positron-lifetime spectra measured after annealing of the samples at temperatures in the range

725–875 K. No direct determination of the He densities in the bubbles is possible, but estimates have been obtained from the bubble sizes found by transmission-electron microscopy[6] (TEM) by assuming the He pressures in the bubbles to be determined by thermal equilibrium.[41] Mean bubble diameters ranged from 40 to 100 Å, depending on the sample. In this size range the interface-state model of the positron is appropriate.

The qualitative agreement between the two sets of points in Fig. 7 is quite good. This firmly establishes the sensitivity of the positron lifetime to gas densities in bubbles. Considering the lack of an absolute density calibration for the experimental data, the theoretical results in Fig. 7 provide the best available relation between helium density and positron lifetime for large helium bubbles in aluminum.

E. Positron calculations for vacancy-He clusters

In the limit of small bubble sizes, which generally corresponds[41] to the highest $\bar{n}_{\text{He}}$, the positron-interface-state model must inevitably break down. The positron will instead be in a volume state extending over the whole bubble volume, and the higher metal electron density in the bubble interior will affect the positron-He interaction to a larger degree than has been assumed so far. For this reason a separate set of calculations has been performed for small He-filled vacancy clusters (consisting of up to 13 vacancies) using the calculational method of Puska and Nieminen.[33] These results are especially relevant to PAT studies of the important initial stages of bubble formation.[42]

The theoretical method is described in detail in Ref. 33. The positron potential is composed of a Coulomb part approximated by atomic superpositions and a correlation potential calculated in a local-density approximation from the electron density (taken as a superposition of atomic densities). No image potential is included and the polarization potential is not included in the positron-He interaction, since this will be screened out by metal electrons in a small vacancy cluster. After numerical solution of the positron Schrödinger equation, the annihilation rate is calculated in a local approximation. The enhancement factor for conduction electrons is approximated by the Brandt-Reinheimer formula,[43] and the independent particle formula (2.9) with the enhancement factor γ equal to 1.5 is used for core electrons.[33,44] Because of the metal-electron screening of the positron-He interaction the He electrons are treated as core electrons equivalent to the metallic core electrons, i.e., the value of γ in the annihilation rate formula (2.9) is 1.5 rather than the 2.9 used in the surface calculations (Sec. II B).

The He positions in the vacancy clusters were chosen so that the symmetry of the cluster was retained compared to the empty cluster, while the He positions still appear physically sound (i.e., filling out the empty space of the vacancy cluster in a reasonable way). The requirement of symmetry is necessary to keep the unit cell of the positron calculation at a computationally manageable size. Exact He locations were determined by minimizing the sum of Al-He and He-He interatomic in-
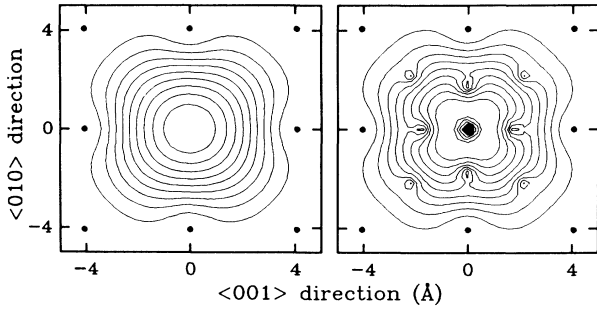
FIG. 9. Calculated positron wave function in an empty 13-vacancy cluster (left) and in a cluster of 13 vacancies and 27 He (right), both in Al. In both cases the contour spacing is $\frac{1}{10}$ of the maximum value. Al atomic positions are indicated by solid circles. The He positions in the right-hand part of the figure can be deduced from the dips in the wave function. Only nine of the He atoms are in the plane of the figure.

teraction energies with respect to one or several parameters defining the He positions under the chosen symmetry restrictions. The Al-He potential in these calculations included only the repulsive effective-medium part and not the van der Waals contribution (see the description of the Al-He potential used in the MD simulations in Sec. II A). The Aziz potential[20] was used for He-He. No relaxations of Al atomic positions were taken into account.

In Fig. 9 wave functions for an empty and a He-filled vacancy cluster are shown. Notice that despite the large He content of the cluster, the overall shape of the wave function is the same in the two cases. As in the surface case (see Sec. II B, especially Fig. 3) the He changes the wave function only locally around each He atom.

Figure 10 shows the calculated lifetimes for a variety of He-vacancy clusters. The results have been grouped according to the ratio between He and vacancy numbers,
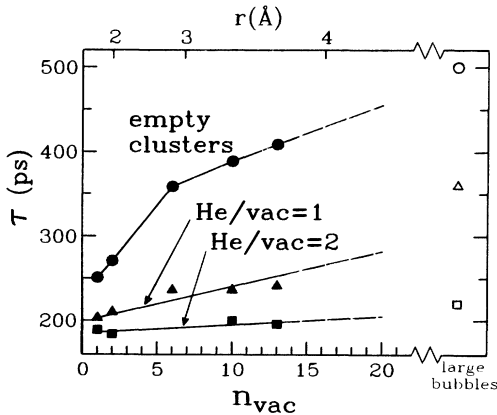

FIG. 10. Calculated lifetimes in empty and He-filled vacancy clusters in Al grouped according to the He-vacancy ratio. The results are shown as a function of the number of vacancies in the cluster, and the upper scale shows the corresponding cluster radius (calculated from the volume of the cluster). The open symbols at the right-hand side of the figure are results for large bubbles obtained from the Fig. 7 relation.

and are displayed as functions of the vacancy number. For all systems in Fig. 10, the positron is strongly bound to the cluster (calculated binding energies relative to bulk range from 1.4 eV upwards). We limit ourselves to clusters with a vacancy number of 13 or less, since the image effects, eventually leading to the transition from a volume to a surface state for increasing cavity size, are not considered in the cluster calculations.

On the right-hand side of Fig. 10 lifetimes for large bubbles from the relation in Fig. 7 are shown for He densities corresponding to the He-vacancy ratios applied in the cluster calculations. As expected, the cluster lifetimes show a trend to approach the large-bubble limit as cluster sizes increase. For the He-vacancy ratio of 2 (corresponding to $\bar{n}_{He} = 1.2 \times 10^{23}$ cm^{-3}) the variation of the lifetime with cavity size appears to be rather small, from ~ 190 ps for the smallest clusters to ~ 220 ps for a large bubble. The results in Fig. 10 show that an observed increase in the lifetime of positrons trapped in small vacancy-He clusters, e.g., upon annealing, can result both from an increase in the cluster sizes and from a decrease in the He-vacancy ratio.

III. METHODS AND RESULTS: Cu-Kr

A. Molecular-dynamics simulations

The geometry used is identical to that used for the Al-He simulations, i.e., six (001) planes of Cu atoms are sandwiched between two sets of Kr atoms in a box with periodic boundary conditions. Particle numbers ranged between 192 and 432 for Cu and between 216 and 512 for Kr.

The Lennard-Jones[45] and Morse[27] potentials were used for the Kr-Kr and Cu-Cu interactions with truncation distances of 7 and 6 Å, respectively. The Cu-Kr potential was described by Eqs. (2.1)–(2.3) and was truncated at 7 Å. The value of 900 eV a_0^3 was used for α_{eff} in Eq. (2.2).[46] The constants in Eq. (2.3) were assigned the values $C = 49.4$ eV Å^6, $r_1 = 1.84$ Å, and $k = 0.25$ Å^{-1}. With these parameters the Kr-surface potential has the correct van der Waals limit[24] and the physisorption well is of depth ~ 0.1 eV about 3.5 Å from the surface. These values are close to those derived from experiments for Kr on Ag(111),[47] while the nearly identical heats of adsorption for Kr on Cu(110) (Ref. 48) and Ag(111) (Ref. 47) indicate that the Kr potentials at Cu and Ag surfaces are similar. The shape of the potential is in good agreement with the proposed universal shape.[26]

The MD time step was 5×10^{-15} s and individual simulations comprised from 500 up to 4000 time steps.

The Kr densities $\bar{n}_{Kr}$ ranged from 1.1 to 3.5×10^{22} cm^{-3}. The simulations were carried out for $T = 300$ K. In addition, for selected densities other temperatures (100 K $< T <$ 1000 K) were also used (the combinations chosen are given in Table I). The initial Kr positions were arranged in a fcc lattice with (001) planes parallel to the metal surface. At high densities (pressures) the Kr remained solid after equilibrium had been obtained, while at lower densities a fluidlike profile developed at the interface. Figure 11 shows examples of these two

TABLE I. Positron results for Cu-Kr interfaces at different Kr densities, $\bar{n}_{Kr}$, and temperatures, T. λ_{Kr} is the annihilation rate with Kr electrons, τ the lifetime [given by $(\lambda_{Kr} + \lambda_{Cu})^{-1}$], and E_b the binding energy to the interface with respect to the vaccum.

$\bar{n}_{Kr}$ (10^{22} cm^{-3})	T (K)	λ_{Kr} (ns^{-1})	τ (ps)	E_b (eV)
1.1	300	0.53	395	3.3
1.8	300	1.15	319	3.5
2.5[a]	300	1.71[c]	269	3.6
2.5[b]	300	1.89[c]	257	3.5
3.5	300	3.41[c]	185	3.5
1.8	100	1.05	328	
1.8	500	1.14	318	
1.8	700	1.19	313	
2.5	700	1.76	266	
2.5	1000	1.96	253	

[a]Geometry corresponding to Fig. 11(b).
[b]Geometry corresponding to Fig. 12(e).
[c]Values calculated by the multilayer method. The other λ_{Kr} values were all obtained by the additivity method.

types of behavior. The observed general features of the phase diagram are in agreement with bulk Kr thermodynamical data.[49,50]

A second type of MD simulation, which corresponds to an idealized "quenching" experiment, was also performed for a Kr density of 2.5×10^{22} cm^{-3}. After the equilibrium density profile had been obtained at a high temperature ($T = 1000$ K), the particle velocities were scaled to correspond to a lower temperature ($T = 300$ K). The evolution of the system was then followed as a function of time, while the simulation temperature was maintained at 300 K. Figure 12 shows the distribution of Kr
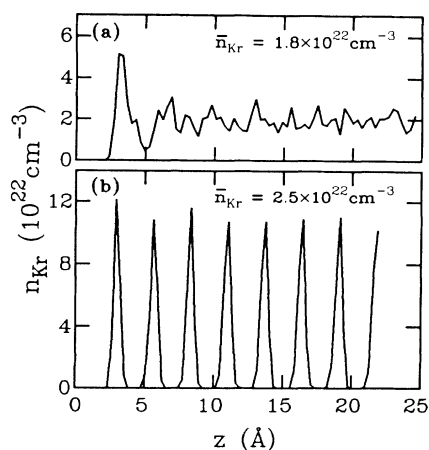

FIG. 11. One-dimensional Kr density profiles perpendicular to the Cu(001) surface obtained by molecular-dynamics simulations. The outermost Cu layer is at $z=0$. In both (a) and (b) the simulation temperature was 300 K. The profiles, which are averaged over 1 ps (200 time steps), correspond to the equilibrium attained after the Kr at the beginning of the simulation was in a solid lattice. In (a) a fluidlike profile has developed, while in (b) the original array of (001) planes is retained.
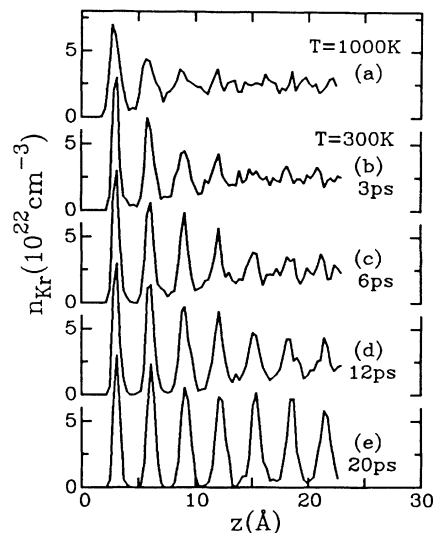

FIG. 12. One-dimensional Kr density profiles perpendicular to the Cu(001) surface obtained by molecular-dynamics simulations. The Kr density is 2.5×10^{22} cm^{-3}. The profile in (a) corresponds to a temperature of 1000 K. In (b)-(e) profiles after a sudden reduction of the temperature from 1000 to 300 K are shown at increasing times after the temperature reduction. All profiles are averaged over the last picosecond (200 time steps) before the time indicated.

perpendicular to the Cu surface as a function of time in this simulation. One clearly sees the development of a solid structure initiated at the Cu-Kr interface. The spacing between layers corresponds to that between close-packed planes at the given Kr density. Within the planes a tendency towards hexagonal-close-packed ordering was observed. The geometry thus shows a change in orientation of lattice planes compared to Fig. 11(b), where the initial array of (001) planes parallel to the metal surface is retained.
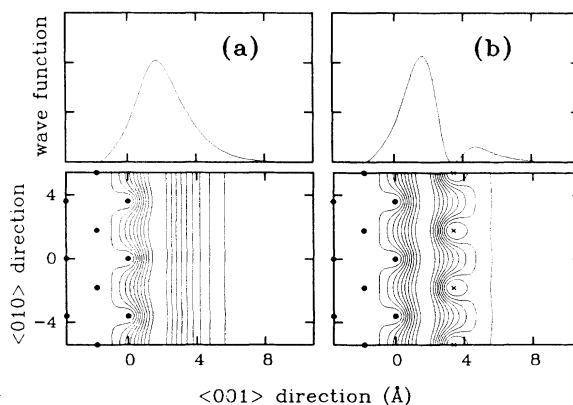

FIG. 13. Positron wave functions at (a) a clean Cu(001) surface and (b) Cu(001) with half a monolayer of Kr at fourfold sites in a $c(2\times2)$ structure. In (b) Kr positions are shown by crosses. The plane of the figure is a (100) plane with all fourfold sites occupied by Kr atoms [every second (100) row of fourfold sites is empty for a $c(2\times2)$ geometry].

B. Positron surface-state calculations: Single Kr layers

The model and methods used for the Cu-Kr interface positron calculations are identical to those used for Al-He described in Sec. II. All calculations were done for the Cu(001) surface. The parameters in the positron-Kr polarization potential, Eq. (2.7), were chosen as $\alpha = 16.74a_0^3$ and $r_0 = 2.37a_0$ (Ref. 32). A value of 3.95 was used for the enhancement factor γ in Eq. (2.9). This number has been determined in a bulk Kr calculation[13] assuming a solid Kr lifetime of 400 ps.

Calculations for single Kr layers were made for half-monolayer coverage in a $c(2 \times 2)$ structure and for a $p(2 \times 2)$ quarter-monolayer (calculations for the physically unrealistic full-monolayer coverage will not be described). In all cases the Kr was positioned at fourfold sites. The distance z_{Kr} between the outermost Cu and the Kr layers was varied between 1.9 and 4.9 Å.

Positron wave functions for clean and Kr covered surfaces are shown in Fig. 13. As in the case of the Al-He system, the positron wave function is not changed considerably in the region where the major positron-metal electron overlap takes place. Thus the calculations predict that the contribution, λ_{Cu}, from Cu electrons to the annihilation rate is close to that for a clean surface, this being around 2 ns^{-1} (Ref. 51). Figure 14 shows the positron binding energy E_b as a function of z_{Kr}. In Fig. 15 the corresponding contributions from Kr electrons to the annihilation rate, λ_{Kr}, are shown. One observes that λ_{Kr} is proportional to coverage, indicating an additivity of λ_{Kr}, similar to that found for λ_{He} in Sec. II. Figure 14 demonstrates that E_b is increased by Kr adsorption compared to the clean-surface value, $E_b^0 = 2.76$ eV, as in the Al-He case. However, for $z_{Kr} > 3$ Å, E_b is about the same for $\Theta = 0.25$ and 0.5, while for smaller z_{Kr}, E_b is *higher* for $\Theta = 0.25$ than for $\Theta = 0.5$.

C. Positron results for the Cu-Kr interface

In the evaluation of λ_{Kr} for a positron trapped at a Cu-Kr interface, two distinct methods, both employing
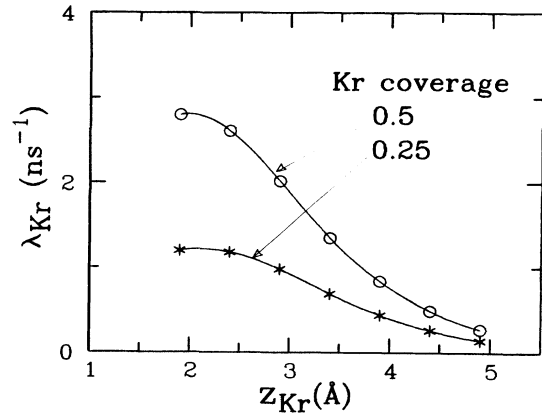
FIG. 15. Annihilation rate with Kr electrons for the same systems as in Fig. 14.

the density profiles obtained by the MD simulations, were used. One method makes use of the additivity approach [i.e., the Kr equivalent of Eq. (2.10) based on positron results for single Kr layers (Fig. 15)]. The other, which will be described below, is based on positron calculations with multiple Kr layers at the Cu surface. The latter method allows an evaluation of the combined effect of the Kr profile on the positron wave function. Eventually, the two methods yielded nearly identical λ_{Kr} values, showing that the local approximation for λ_{Kr} inherent in the additivity method is indeed valid for all Kr profiles considered, and the overall shape of the positron wave function, disregarding the changes occurring in the regions close to Kr atomic positions, is not changed by the introduction of more than one Kr layer at the surface. Thus the conclusion inferred from the single-layer results, that λ_{Cu} is equal to the clean-surface value, remains valid in the multilayer geometry and, consequently, also in a real interface geometry. Moreover, it is found that by far the largest contribution ($> 80\%$) to λ_{Kr} comes from the very first Kr layer at the interface, the other layers playing only a secondary role.

The multiple-layer method exploits the fact that in many cases [e.g., Figs. 11(b) and 12(e)] the Kr is distributed in well-defined layers, each corresponding to a certain coverage. For each MD Kr profile the coverage per Kr layer, Θ_1, and the layer positions, were determined. Two positron surface calculations with (ordered) Kr layers at these positions were then made, one with $\Theta_1 = 0.25$ and one with $\Theta_1 = 0.5$ (since the layer positions are different for different profiles, a set of positron calculations had to be made for each separate case). The annihilation rate λ_{Kr} for the interface was then found by scaling the λ_{Kr} values found in the calculations to the true Θ_1, which for the various profiles considered ranged from 0.30 to 0.56. Since the calculations indicate proportionality of λ_{Kr} with Θ_1 in all cases (λ_{Kr} approximately doubled when going from $\Theta_1 = 0.25$ to $\Theta_1 = 0.5$), this scaling is legitimate.

Table I gives the calculated λ_{Kr} values for positrons trapped at Cu-Kr interfaces. Calculations of λ_{Kr} by the multilayer method just described were made for all sys-
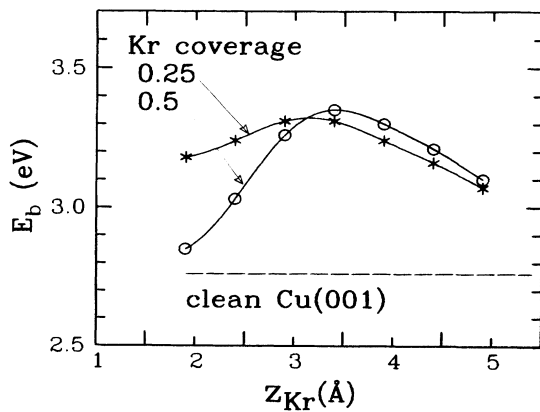

FIG. 14. Binding energy with respect to vacuum of a positron at a Cu(001) surface covered by a single Kr layer as a function of the surface-Kr distance. The Kr coverage is indicated for each set of results. The clean Cu(001) binding energy is shown as the horizontal dashed line.

tems at 300 K, but the additivity method results were preferred at the two lowest densities, since in these cases the Kr profile was fluidlike [cf. Fig. 11(a)] rather than divided into layers. For the lowest density the deviation between multilayer and additivity λ_{Kr} values is 16%, while in the other cases it is less than 6%. The lifetime values given in the fourth column of Table I have been calculated as $\tau=(\lambda_{Cu}+\lambda_{Kr})^{-1}$ with λ_{Cu} equal to 2.0 ns^{-1}. One observes that the two different geometries considered for $\bar{n}_{Kr}=2.5\times10^{-22}$ cm^{-3} and $T=300$ K yield lifetimes in close agreement, and that the effect of temperature on the lifetime at a given $\bar{n}_{Kr}$ appears to be small. The calculated lifetime values for $T=300$ K have been plotted against Kr density in Fig. 16. The relation between τ and n_{Kr} is observed to be very nearly linear, in correspondence with the τ-versus-$\bar{n}_{He}$ relationship in Fig. 7. The relation can be expressed as

$$\tau(ps)=500-92.3\bar{n}_{Kr}(10^{22}\ cm^{-3})\ . \qquad (3.1)$$

Experimental support for the calculated relation is presented in the following subsection.

The binding energies in the last column of Table I were all obtained from the multilayer calculations. In each set of explicit calculations the E_b values for $\Theta_1=0.25$ and 0.5 agreed within 0.2 eV. The value for the genuine Θ_1 was found by interpolation or extrapolation based on these values. The binding energy is increased compared to the clean surface (2.76 eV), but shows very little variation with $\bar{n}_{Kr}$.

D. Comparison with experiment

In the τ-versus-$\bar{n}_{Kr}$ graph, Fig. 16, an experimental point is included. This has been obtained from Cu samples containing about 3 at.% krypton.[9,10,52] In these samples Kr has been shown[53] to be present in bubbles containing solid krypton. The lifetime, $\tau=257$ ps, is the longest lifetime component for the as-prepared samples.
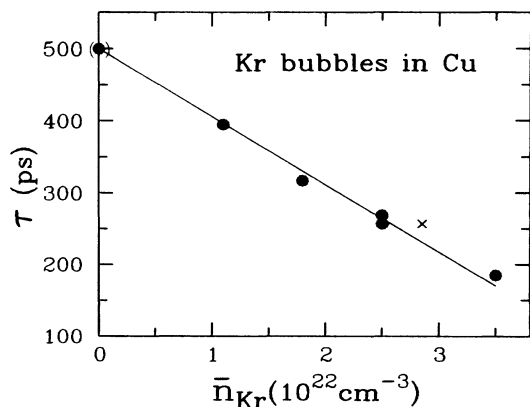

FIG. 16. Positron lifetime as a function of Kr density in Kr bubbles in Cu at 300 K. Solid circles denote theoretical interface results (data from Table I). The line drawn is a visual fit. The cross is an experimental point for Cu containing ~3 at.% Kr (see text).

The corresponding density estimate has been obtained from the lattice parameter of the Kr lattice in the bubbles determined by electron diffraction on samples similar to those used for positron measurements (a density estimate based on the macroscopic swelling and the estimated Kr content of the samples gives approximately the same value[54]). The agreement between the theoretical τ-versus-$\bar{n}_{Kr}$ relation and the experimental result is encouraging.

Experimental results are also available[10,52] for Kr in Ni. For Ni containing ~5 at.% Kr a lifetime of 243 ps is measured,[52] while the Kr density estimated from the electron-diffraction lattice parameter[53] is 3.20×10^{22} cm^{-3}. No explicit calculations have been done for Ni-Kr, but a τ-versus-$\bar{n}_{Kr}$ relation similar to that for Cu-Kr is to be expected (see Sec. IV A). Comparison between the theoretical relation of Fig. 16 and the Ni-Kr data reveals a fair agreement supporting this idea.

E. Positron calculations for vacancy-Kr clusters

The course of the positron calculations for Kr-filled vacancy clusters in Cu (and Ni) closely follows that of the Al vacancy-He cluster calculations—see Sec. II E.

Equivalent to the He case, the positron-Kr polarization interaction is not included in the positron potential, and the Kr electrons are treated as the metal core electrons with $\gamma=1.5$ in the calculation of the annihilation rate. The annihilation with Cu d electrons is calculated using the independent-particle formula (2.9) with enhancement γ_d equal to 1.76. This number has been adjusted to reproduce the bulk Cu lifetime correctly.[33]

Kr positions in the clusters were determined by an energy minimization scheme identical to that used for Al-He. No attractive part was included in the Cu-Kr potential in these calculations, and relaxations of Cu positions were not considered.

In Table II the calculated lifetimes for vacancy-Kr clusters in Cu are given. Results for Ni-Kr obtained by the same procedure as the Cu-Kr results are also shown. The calculated positron binding energies are larger than 1.5 eV for all clusters in Table II. The calculated lifetimes in Ni are systematically about 12 ps smaller than the corresponding Cu values. This will presumably also apply for the Ni-Kr clusters, for which no explicit calculations were made.

Table II shows that the introduction of a single Kr atom into a vacancy cluster reduces the positron lifetime considerably, as has already been demonstrated by Hansen et al.[13] Subsequent Kr atoms have a less drastic effect since the mutual repulsion of Kr atoms disfavors Kr positions near the cluster center, where the positron wave function in the empty cluster has its maximum. At high Kr-vacancy ratios of about 1/3, lifetimes around 220 ps are calculated for clusters in Cu (Table II). This is close to the value calculated for large bubbles in the interface model of 241 ps at the equivalent Kr density of 2.8×10^{28} m^{-3}, cf. Fig. 16. As in the Al-He case, cf. Fig. 10, it thus appears that the influence of size effects on the lifetime is small at high gas densities. At lower Kr densities size effects are seen to be more important.

TABLE II. Positron lifetimes (in ps) for vacancy-Kr clusters in Cu and Ni for different combinations of vacancy and Kr numbers.

Number of vacancies	Number of Kr atoms			
	0	1	2	4
Cu				
4	276	181	178	
6	310	212	220	
10	346	262	237	223
13	372	284		229
Ni				
4	264	169	166	
13	364	271		217

IV. DISCUSSION

A. Generalization of the positron results

We have in the preceding sections considered the trapping of positrons at metal–noble-gas interfaces. Explicit calculations were made for the Al-He and Cu-Kr systems. However, one might, on very general terms, expect relations between the positron lifetime and $\bar{n}_{He}$ and $\bar{n}_{Kr}$ qualitatively similar to those for Al and Cu, respectively, also for other metals. The gas-density profiles are mainly determined by the extension of the electron distribution outside the surface, i.e., the "size" of the metal atoms, which for many metals is roughly the same, while the positron surface states at different metal surfaces also appear to be similar (same E_b within about 1 eV, Ref. 38), suggesting positron-gas overlaps for various interfaces to be alike. This notion is supported by the agreement between the single result obtained for the Cu-He system and the Al-He results (Sec. II C), and by the comparison between the experimental results for the Ni-Kr system with the lifetime–Kr-density relation derived for Cu-Kr (Sec. III D).

The theoretical calculations have all been performed for planar surfaces corresponding to the surface facets of large gas bubbles. When considering real bubbles, one can, however, not exclude the possibility of surface imperfections. It is conceivable that vacancy-type interfacial defects or other imperfections such as steps and kinks can trap positrons, which in the present model are delocalized along the interface. We have not examined this possibility explicitly in the calculations. However, the contours of both positron-surface and gas-surface potentials, which in turn determine the positron and fluid densities, follow the electron-density contours at the surface. This is a consequence of the corrugated mirror model for the positron and the effective-medium formula [Eq. (2.2)] for the gas atoms [for the present argument the attractive part of the gas-surface potential, Eq. (2.3), can be neglected]. The changes in positron and gas densities induced by surface imperfections therefore tend to *match*. Consequently, the positron-electron overlap and, hence, λ_{gas} will be relatively insensitive to details in the surface geometry. It is difficult to quantify this general statement, but the qualitative effect, namely that the pos-

itron lifetime is directly related to gas densities inside bubbles, is unlikely to be disturbed by the presence of imperfections.

In the theoretical description of the positron interface state employed, the positron–gas-atom interaction is assumed to be unaffected by the metal electrons, since the gas-atom positions are almost exclusively in the image-potential region (distances from the topmost surface layer greater than about 2 Å, cf. Figs. 1 and 11), where no accumulation of metal electrons around the positron occurs. In the "physisorbed Ps" picture[55] of the positron surface state, one would expect a stronger screening of the positron–gas-atom interaction, and accordingly a smaller overlap leading to a lower λ_{gas} rather like an ortho-Ps pick-off annihilation rate.[39] In this picture it would be difficult to account for the observed lifetimes without assuming unrealistically high gas densities in the bubbles. The image-potential model thus appears to provide a better description of the positron surface (interface) state in gas bubbles than the Ps model.

B. Application to positron experiments

As noted in the Introduction the calculations were originally motivated by a number of positron experiments on metals systems containing gas bubbles. Examples of the application of the theory in the interpretation of experiments are given in the following. Extended discussions are provided in the papers describing the experiments in question.

Experiments on He bubbles in (600–800)-MeV-proton–irradiated Al (Ref. 6) have already been mentioned in Sec. II D as providing independent support of the theoretical lifetime He-density relation. Defect-associated lifetimes in samples irradiated below 420 K in the as-irradiated state are in the range 300–350 ps. With Eq. (2.11) this corresponds to He densities around 7×10^{22} cm^{-3}. This value for the He density inside bubbles is quite realistic.[14] Upon annealing, the positron lifetime in the defects increases when the annealing temperature exceeds ~ 600 K (Ref. 6), which implies a decrease in the He density. Very similar results have been reported for He-irradiated Al.[7] When the density information obtained from Eq. (2.11) is supplemented with information on trapping rates of positrons into the bubbles and the total He content in the samples, quantitative es-

timates of bubble sizes and concentrations as a function of annealing temperature can be made, in good agreement with corresponding transmission-electron-microscopy (TEM) data.[56] An important piece of information provided by the theory is that the lifetimes observed can be accounted for by the He bubbles known from TEM investigations to be present without having to postulate the presence of small (invisible) vacancy clusters.[57]

The results for Cu and Ni containing Kr at atomic percent concentrations[9,10,52] were shown in Sec. III D to give supportive evidence for the theory. The increase in defect lifetime (which eventually reached 450–500 ps) observed as samples were annealed[10,52] indicates a decrease in Kr density inside the bubbles. The Kr densities estimated with the use of Eq. (3.1) after annealing at different temperatures agree well with densities estimated from electron-microscopy data by assuming bubbles to be in thermal equilibrium.[52] The results in Table II have mainly been applied to define the extent to which small vacancy-Kr clusters (invisible in TEM), as opposed to the large bubbles, are able to account for the observed PAT results.[52]

The results have so far been discussed in relation to gas bubbles in metals. However, they will also apply to other cases, such as when noble gases are adsorbed on (external) metal surfaces.[58] For Kr on Cu, Figs. 14 and 15 show that a single Kr layer at the saturation coverage of about 0.40 positioned at the physisorption distance around 3.5-Å causes an increase in binding energy of a surface trapped positron by about 0.5 eV and a decrease of the lifetime from ~500 ps to ~300 ps. Subsequent Kr layers have little effect beyond that caused by the first layer, since these layers are quite far from the surface compared to the extension of the positron surface state. Since the positron work function of Kr (1.7 eV, Ref. 58) is smaller than the positron binding energy to the surface (interface), ~3 eV, the interface-trapped state is the lowest energy state in Cu-Kr systems. This, presumably, also applies to other metal–noble-gas systems.

The large change in the lifetime of a surface-trapped positron when a Kr layer is condensed at the surface can be used to detect the presence of Kr in bubbles even when the Kr density is so low that the lifetime at 300 K is indistinguishable from the empty-void lifetime (cf. Fig. 16). When the temperature is lowered sufficiently, a clear reduction in the lifetime should be observed when the Kr starts to condense at the bubble surface. This effect has recently been observed[59] for the Cu-Kr samples mentioned above after annealing treatments had increased bubble sizes and reduced the Kr density inside. The magnitude of the lifetime decrease observed upon cooling of the samples appears to be consistent with the theoretical estimates. Since the temperature at which the condensation of the first layer occurs depends on the Kr pressure,[47] measurement as function of temperature should, in principle, be able to yield information about the Kr density. Even if it is not possible to quantify this information, the mere detection of the presence of gas in the cavities would be valuable in many cases.

C. Solidification of gas bubbles

Electron diffraction studies have established that heavy noble gases (Ar, Kr, Xe), when implanted into metals, precipitate into solid gas bubbles.[53,60–64] These studies have revealed that close-packed planes of the (fcc or hcp) lattice are parallel to close-packed metal lattice planes, even though the metal and gas lattice constants are incommensurate. This holds also for bcc Mo. Recently, Finnis[65] has offered an explanation of this alignment by comparing the interaction energies in the bulk gas and at the gas-metal interface in a geometry where the noble gas is confined between two metallic (plane) surfaces. It was found that an arrangement of gas atoms with close-packed planes parallel to the metallic surface is energetically favorable compared to condensation of the gas with loosely packed planes next to the metal. Since the metallic bubble surfaces are likely to be close packed, this effect can explain the alignment of the gas and metal lattices. In the molecular-dynamics simulations in the present work a direct demonstration of the effect predicted by Finnis[65] is given, since in the "quenching" simulation in Fig. 12 the Kr gas solidifies in planes of close-packed character parallel to the metallic Cu(001) surface.

Let us finally note the possible connection between our MD results and the experimentally observed superheating of solid gas precipitates in metals. Recently, Rossouw and Donnelly[60] reported a solid-fluid transition in Ar in bubbles in Al 480 K above the bulk Ar melting temperature at the density in question. The melting transition was deduced by the disappearance of the electron-diffraction spots associated with the Ar. [The superheating effect is apparently much smaller or even absent for Kr in Cu or Ni (Ref. 53).] Since bubbles, in general, must be small to withstand the high pressures required to solidify the gas at high temperatures, quite a large fraction of the gas atoms will be at the bubble surface. Thus the gas behavior at the gas-metal interface will be of great importance to all bubble properties. Rossouw and Donnelly[60] discuss the surface effects in terms of reduced thermal vibrations of the gas atoms caused by the metal surface, and this is presented as a mechanism for suppression of the melting transition. The present MD results suggest an alternative explanation which may not be described as a true superheating effect, since it does not exclude that in the bubble interior melting takes place at the predicted bulk melting temperature. The peak(s) in the gas-density profiles observed in the MD simulations (see Figs. 1 and 11), even when the bulk gas is fluid, are a signature of ordering processes at the interface, which in a small bubble might yield a solidlike diffraction pattern above the bulk melting point of the gas. It would be interesting to pursue this topic by doing MD simulations with a geometry corresponding to a real three-dimensional bubble, which would allow direct comparison with experiment.

V. CONCLUSION

The major conclusion which can be drawn from the results in the preceding sections is that the lifetime of a

positron trapped in a noble-gas bubble depends on the gas density in the bubble. This was explicitly demonstrated for the Al-He and Cu-Kr systems, but presumably applies to a wide range of other metal-gas systems as well. The general agreement with experimental evidence indicates that this effect can be utilized in a quantitative density determination. To reach this conclusion a general theoretical framework was developed and it was shown that in large bubbles the positron is trapped at the metal-gas interface. It is our hope that the present work will provide a foundation for the interpretation of positron experiments on metal–noble-gas systems and hopefully will encourage further research in this field, allowing further tests of the adequacy of the theoretical model and possibly suggest refinements or expansions of the theory.

*Present address: School of Mathematics and Physics, University of East Anglia, Norwich NR4 7TJ, United Kingdom.

†Address during 1987: LASSP, Clark Hall, Cornell University, Ithaca, NY 14850.

[1]H. Ullmaier, Nuclear Fusion 24, 1039 (1984).

[2]Proceedings of the International Symposium on Fundamental Aspects of Helium in Metals, edited by H. Ullmaier [Radiat. Eff. 78, 1 (1983)].

[3]R. G. Musket, W. McLean, C. A. Colmenares, D. M. Makowiecki, and W. J. Siekhaus, Appl. Surf. Sci. 10, 143 (1982).

[4]S. Matteson and M-A. Nicolet, Annu. Rev. Mater. Sci. 13, 339 (1983).

[5]C. L. Snead, A. N. Goland, and F. W. Wiffen, J. Nucl. Mater. 64, 195 (1977).

[6]K. O. Jensen, M. Eldrup, B. N. Singh, M. Victoria, and W. V. Green, in Positron Annihilation, edited by P. C. Jain, R. M. Singru, and K. P. Gopinathan (World-Scientific, Singapore, 1985), p. 473; K. O. Jensen, M. Eldrup, B. N. Singh, and M. Victoria (unpublished).

[7]H. E. Hansen, H. Rajainmäki, R. Talja, M. D. Bentzon, R. M. Nieminen, and K. Petersen, J. Phys. F 15, 1 (1985).

[8]G. Kögel, Q.-M. Fan, P. Sperr, W. Triftshäuser, and B. Viswanathan, J. Nucl. Mater. 127, 125 (1985).

[9]M. Eldrup and J. H. Evans, J. Phys. F 12, 1265 (1982).

[10]K. O. Jensen, M. Eldrup, and J. H. Evans, in Positron Annihilation, Ref. 6, p. 506.

[11]Positron Solid-State Physics, edited by W. Brandt and A. Dupasquier (North-Holland, Amsterdam, 1983).

[12]Positrons in Solids, edited by P. Hautojärvi (Springer, Berlin, 1979).

[13]H. E. Hansen, R. M. Nieminen, and M. J. Puska, J. Phys. F 14, 1299 (1984).

[14]S. E. Donnelly, Radiat. Eff. 90, 1 (1985).

[15]K. O. Jensen and R. M. Nieminen, Phys. Rev. B 35, 2087 (1987).

[16]See, e.g., D. W. Heermann, Computer Simulation Methods in Theoretical Physics (Springer, Berlin, 1986).

[17]M. W. Finnis, A. van Veen, and L. M. Caspers, in Ref. 2, p. 121.

[18]L. M. Caspers, A. van Veen, and T. J. Bullough, in Ref. 2, p. 67.

[19]M. W. Finnis and A. H. Harker, Atomic Energy Research Establishment–Harwell Report No. 8824, 1983 (unpublished).

[20]R. A. Aziz, V. P. S. Nain, J. S. Carley, W. L. Taylor, and G. T. McConville, J. Chem. Phys. 70, 4330 (1979).

[21]M. H. Kalos, M. A. Lee, P. A. Whitlock, and G. V. Chester, Phys. Rev. B 24, 115 (1981).

[22]M. Manninen, J. K. Nørskov, M. J. Puska, and C. Umrigar, Phys. Rev. B 29, 2314 (1984).

[23]P. Cremaschi and J. L. Whitten, Surf. Sci. 169, L289 (1986).

[24]E. Zaremba and W. Kohn, Phys. Rev. B 13, 2270 (1976).

[25]P. Nordlander and J. Harris, J. Phys. C 17, 1141 (1984).

[26]G. Vidali, M. W. Cole, and J. R. Klein, Phys. Rev. B 28, 3064 (1983).

[27]L. A. Girifalco and V. G. Weizer, Phys. Rev. 114, 687 (1959).

[28]K. W. Jacobsen, J. K. Nørskov, and M. J. Puska, Phys. Rev. B 35, 7423 (1987); M. W. Finnis and J. E. Sinclair, Philos. Mag. A 50, 45 (1984); M. S. Daw and M. I. Baskes, Phys. Rev. B 29, 6443 (1984).

[29]D. E. Sullivan, D. Levesque, and J. J. Weis, J. Chem. Phys. 72, 1170 (1980).

[30]R. M. Nieminen, in Positron Solid-State Physics, Ref. 11, p. 359.

[31]R. M. Nieminen and M. J. Puska, Phys. Rev. Lett. 50, 281 (1983); M. J. Puska and R. M. Nieminen, Phys. Scr. T 4, 79 (1983).

[32]D. M. Schrader, Phys. Rev. A 20, 918 (1979).

[33]M. J. Puska and R. M. Nieminen, J. Phys. F 13, 333 (1983).

[34]R. M. Nieminen, M. J. Puska, and M. Manninen, Phys. Rev. Lett. 53, 1298 (1984).

[35]K. G. Lynn, W. E. Frieze, and P. J. Schultz, Phys. Rev. Lett. 52, 1137 (1984).

[36]S. Linderoth, M. D. Bentzon, H. E. Hansen, and K. Petersen, in Positron Annihilation, Ref. 6, p. 494; K. Petersen, N. Thrane, G. Trumpy, and R. W. Hendricks, Appl. Phys. 10, 85 (1976); R. M. Nieminen, J. Laakkonen, P. Hautojärvi, and A. Vehanen, Phys. Rev. B 19, 1397 (1979); V. W. Lindberg, J. D. McGervey, R. W. Hendricks, and W. Triftshäuser, Philos. Mag. 36, 117 (1977).

[37]P. Hautojärvi, K. Rytsölä, P. Tuovinen, A. Vehanen, and P. Jauho, Phys. Rev. Lett. 38, 842 (1977).

[38]See, e.g., A. P. Mills, in Positron Solid-State Physics, Ref. 11, p. 432.

[39]K. Rytsölä, J. Vettenranta, and P. Hautojärvi, J. Phys. B 17, 3359 (1984).

[40]R. M. Nieminen and J. Laakkonen, Appl. Phys. 20, 181 (1979).

[41]R. Manzke, W. Jäger, H. Trinkhaus, G. Crecelius, and R. Teller, Solid State Commun. 44, 481 (1982).

[42]H. E. Hansen, H. Rajainmäki, R. M. Nieminen, S. Linderoth, and K. Petersen, in Positron Annihilation, Ref. 6, p. 512.

[43]W. Brandt and J. Reinheimer, Phys. Lett. 35A, 109 (1971).

[44]E. Bonderup, J. U. Andersen, and D. N. Lowy, Phys. Rev. B 20, 883 (1979); K. G. Lynn, J. R. MacDonald, R. A. Boie, L.

C. Feldman, J. D. Gabbe, M. F. Robbins, E. Bonderup, and J. Golovchenko, Phys. Rev. Lett. **38**, 241 (1977).

[45]LJ potential parameters were taken from N. W. Ashcroft and N. D. Mermin, *Solid State Physics* (Holt, Rinehart and Winston, New York, 1976).

[46]M. J. Puska (private communication).

[47]J. Unguris, L. W. Bruch, E. R. Moog, and M. B. Webb, Surf. Sci. **109**, 522 (1981); J. Unguris, L. W. Bruch, M. B. Webb, and J. M. Philips, *ibid.* **114**, 219 (1982).

[48]A. Glachant, M. Jaubert, M. Bienfait, and G. Boato, Surf. Sci. **115**, 219 (1981).

[49]C. Ronchi, J. Nucl. Mater. **96**, 314 (1981).

[50]A. Paskin, A.-M. Llois de Kreiner, K. Shukla, D. O. Welsh, and G. J. Dienes, Phys. Rev. B **25**, 1297 (1982).

[51]M. Eldrup, J. H. Evans, O. E. Mogensen, and B. N. Singh, Radiat. Effects **54**, 65 (1981); G. Kögel, J. Winter, and W. Trifthäuser, in *Positron Annihilation*, edited by R. R. Hasiguti and K. Fujiwara (Japan Institute of Metals, Sendai, 1979), p. 707.

[52]K. O. Jensen, M. Eldrup, N. J. Pedersen, and J. H. Evans (unpublished).

[53]J. H. Evans and D. J. Mazey, J. Phys. F **15**, L1 (1985).

[54]J. H. Evans, R. Williamson, and D. S. Whitmell, in *Effect of Radiation on Materials: 12*th *International Symposium*, edited by F. A. Garner and J. S. Perrin (American Society for Testing and Materials, Philadelphia, 1985), p. 1225.

[55]P. M. Platzman and N. Tzoar, Phys. Rev. B **33**, 5900 (1986).

[56]K. O. Jensen, M. Eldrup, B. N. Singh, A. Horsewell, M. Victoria, and W. F. Sommer, Mater. Sci. Forum **15-18**, 913 (1987).

[57]P. Jena and B. K. Rao, Phys. Rev B **31**, 5634 (1985).

[58]E. M. Gullikson and A. P. Mills, Phys. Rev. Lett. **57**, 376 (1986).

[59]K. O. Jensen, M. Eldrup, S. Linderoth, and J. H. Evans (unpublished).

[60]C. J. Rossouw and S. E. Donnelly, Phys. Rev. Lett. **55**, 2960 (1985).

[61]A. Vom Felde, J. Fink, Th. Müller-Heinzerling, J. Pflüger, B. Scheerer, G. Linker, and D. Kaletta, Phys. Rev. Lett. **53**, 922 (1984).

[62]C. Templier, C. Jaouen, J.-P. Rivière, J. Delafond, and J. Grilhé, C. R. Acad. Sci. Paris **299**, 613 (1984).

[63]J. H. Evans and D. J. Mazey, Scr. Metall. **19**, 621 (1985).

[64]J. H. Evans and D. J. Mazey, J. Nucl. Mater. **138**, 176 (1986).

[65]M. W. Finnis, Acta Metall. **35**, 2543 (1987).